

Supporting Information:

Multi-modal, ultrasensitive, wide-range humidity sensing with Ti_3C_2 film

Eric S. Muckley¹, Michael Naguib², Iliia N. Ivanov^{1*}

¹Center for Nanophase Materials Sciences, Oak Ridge National Laboratory, P.O. Box 2008, Oak Ridge, Tennessee 37831, USA

²Department of Physics and Engineering Physics, Tulane University, New Orleans, Louisiana 70118, USA

Film morphology

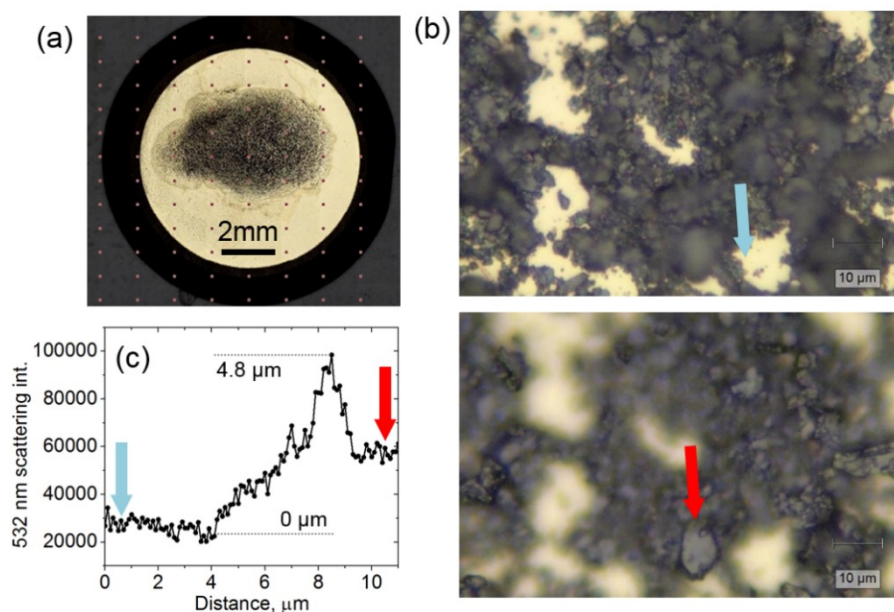


Figure S1. (a) Optical microscope image of Ti_3C_2 film deposited on Au-coated QCM crystal. Using the Au surface as a reference ((b) top panel), the scattering intensity of a 532 nm laser and adjustable microscope focus were used to estimate height of domains ((b) bottom panel). (c) A line profile measured from blue to red arrows in (b) shows that the largest domains are $\sim 5 \mu\text{m}$ in diameter.

Long-term stability and reproducibility

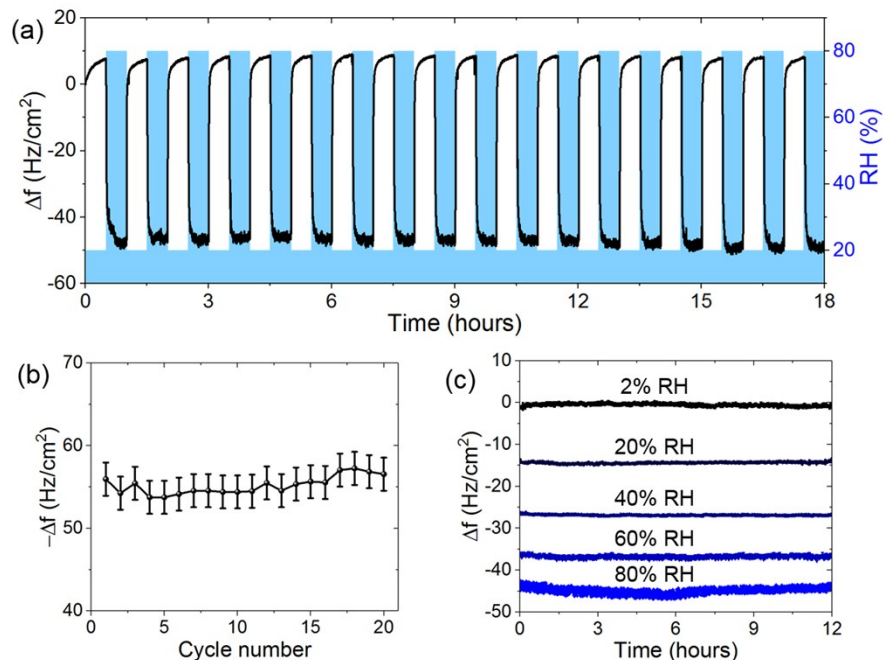


Figure S2. (a) Gravimetric response of Ti₃C₂-coated QCM (black, left axis) during 18 hours of repeated cycling from 20% to 80% RH (blue, right axis). (b) Response during cycling remained constant within 6% over the 18 hour, 20-cycle experiment. (c) Gravimetric response during constant RH showed stability over 12 hours.

Electrical impedance spectroscopy

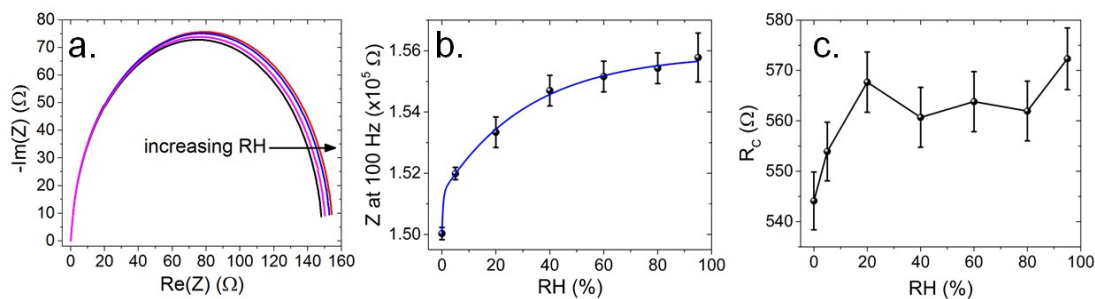


Figure S3. (a) Nyquist representation of spectroscopic impedance shows that largest impedance increases with RH occur at low frequency (~ 100 Hz). (b) Impedance measured at 100 Hz increases with RH and follows a roughly double exponential trend (blue line). Error bars correspond to signal to noise ratio measured at each RH step. (c) Contact resistance (R_c) extracted from equivalent circuit model shows slight increase with RH. Error bars correspond to quality of fits to equivalent circuit.

Quartz crystal microbalance with dissipation monitoring

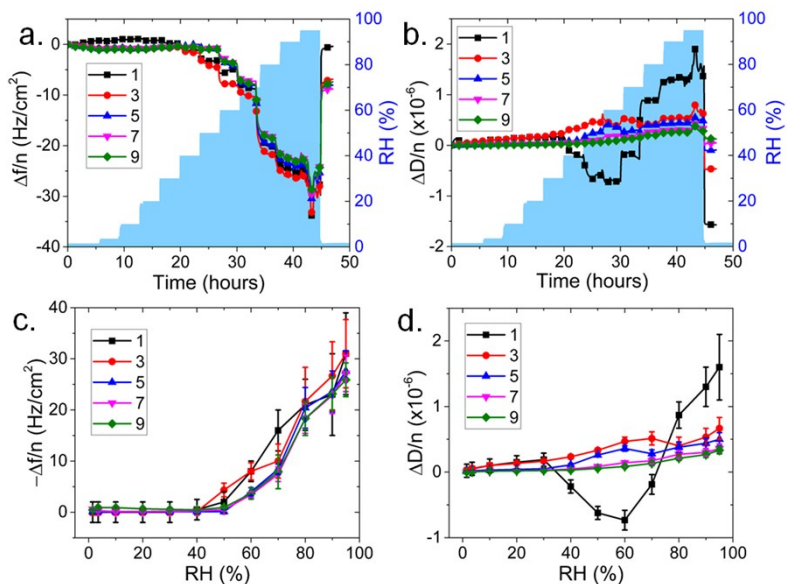


Figure S4. (a) Frequency shift normalized to harmonic number ($\Delta f/n$) of bare Au QCM during exposure to increasing RH (blue, right axis). Legend shows crystal harmonic number. (b) Change in dissipation normalized to harmonic number ($\Delta D/n$) of bare Au QCM during exposure to increasing RH. (c) Magnitude of $\Delta f/n$ vs RH. (d) Magnitude of $\Delta D/n$ vs RH.

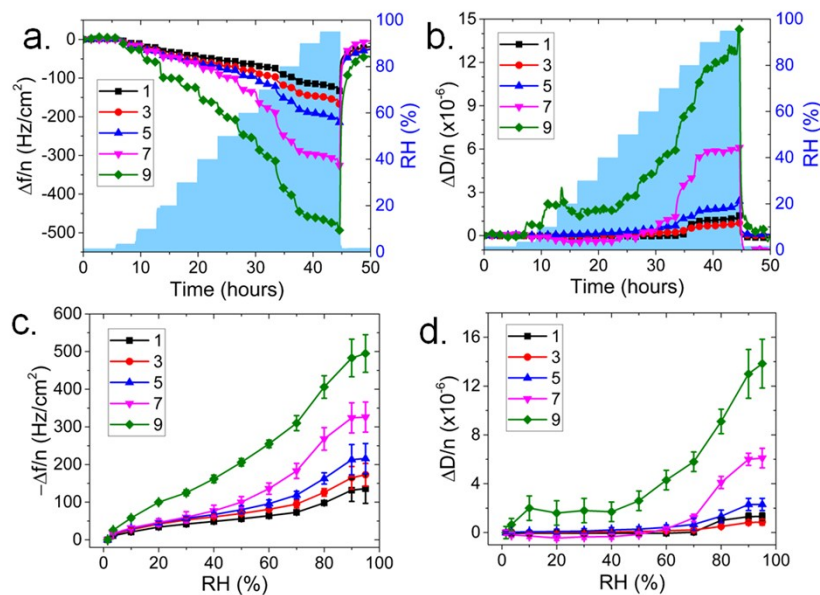


Figure S5. (a) Frequency shift normalized to harmonic number ($\Delta f/n$) of Ti₃C₂-coated QCM during exposure to increasing RH (blue, right axis). Legend shows crystal harmonic number. (b) Change in dissipation normalized to harmonic number ($\Delta D/n$) of Ti₃C₂-coated QCM during exposure to increasing RH. (c) Magnitude of $\Delta f/n$ vs RH. (d) Magnitude of $\Delta D/n$ vs RH.

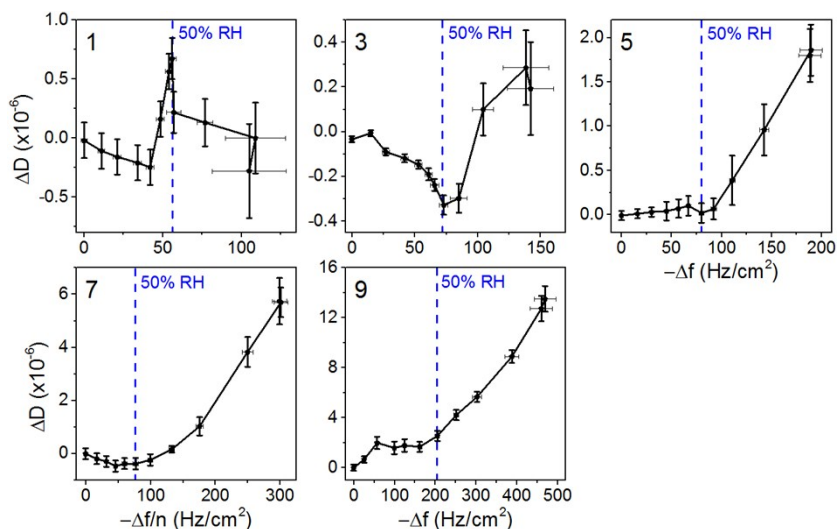


Figure S6. Change in dissipation vs. frequency shift of Ti_3C_2 -coated QCM measured at odd crystal harmonics during exposure to increasing RH. Harmonic number is shown in upper left corner of each panel. Error bars correspond to noise amplitude in Δf and ΔD measurements. Values of Δf and ΔD from bare Au QCM have been subtracted to remove effects of H_2O adsorption on Au and changing viscosity of air. Blue dashed line in each panel shows 50% RH level, where rough transitions in slope of ΔD vs. Δf are observed. Points to the left side of the dashed line correspond to $\text{RH} < 50\%$ and points to the right side of the dashed line correspond to $\text{RH} > 50\%$.

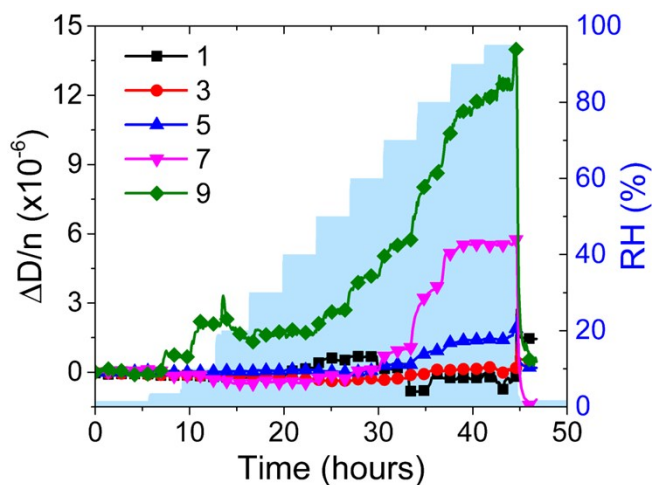


Figure S7. Dissipation ($\Delta D/n$) normalized to harmonic number of Ti_3C_2 -coated QCM during exposure to increasing RH levels (blue, right axes). Values of $\Delta D/n$ for bare Au QCM (Figure S4) were subtracted to remove effects of water adsorption on Au and drag forces arising from changing density and viscosity of humid air. Legend shows crystal harmonic number.

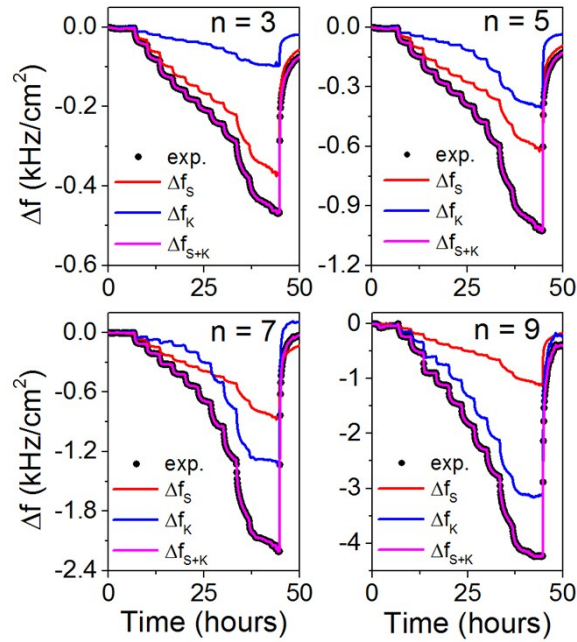


Figure S8. Modelling of frequency shift using contributions from linear Sauerbrey (Δf_S) and nonlinear Kanazawa-Gordon (Δf_K) models to fit values measured experimentally. The sum of Sauerbrey and Kanazawa contributions (Δf_{S+K}) fits the experimental data and enables extraction of mass change and viscoelastic change in the adlayer film. Harmonic number is shown in the upper right-hand corner of each panel.

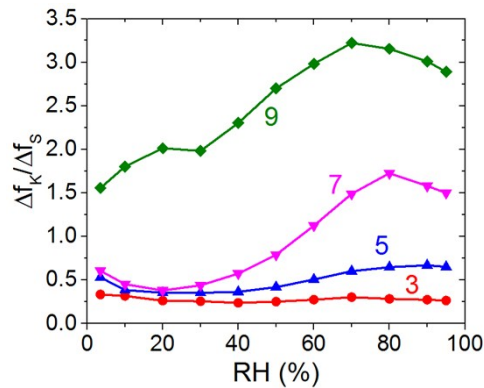


Figure S9. Ratio of frequency shift attributed to nonlinear viscous effects as described by Kanazawa (Δf_K) to that of linear effects described by Sauerbrey (Δf_S). Colored numbers correspond to harmonic number,

Viscoelastic modelling of Ti₃C₂ film

Mechanical properties of an adlayer film deposited on QCM can be characterized by introducing a shear viscosity coefficient (η) and a shear elasticity modulus (μ) through use of the well-known Voigt model. Using the approach of Voinova et al. for modelling response of film with non-negligible viscoelastic properties in a low-viscous fluid (air or vacuum)¹, Δf and ΔD are related to η , μ , and the film density (ρ) by

$$\Delta f \approx \frac{-1}{2\pi\rho_Q h_Q \sqrt{2}} \left(\eta\omega \sqrt{\frac{\mu^2 + \eta^2\omega^2 + \mu}{\mu^2 + \eta^2\omega^2}} - \mu \sqrt{\frac{\mu^2 + \eta^2\omega^2 - \mu}{\mu^2 + \eta^2\omega^2}} \right) \quad (1)$$

$$\Delta D \approx \frac{1}{\pi f_0 \rho_Q h_Q \sqrt{2}} \left(\eta\omega \sqrt{\frac{\mu^2 + \eta^2\omega^2 - \mu}{\mu^2 + \eta^2\omega^2}} + \mu \sqrt{\frac{\mu^2 + \eta^2\omega^2 + \mu}{\mu^2 + \eta^2\omega^2}} \right) \quad (2)$$

where ρ_Q and h_Q are density and thickness of the quartz oscillator respectively and $\omega = 2\pi f$ is the angular frequency. For modelling the viscosity and shear modulus of the film under changing RH conditions, we fixed film density $\rho = 2 \text{ g/cm}^3$, in agreement with previously reported densities for Ti₃C₂ films²⁻³. Using Δf and ΔD values shown in Figure 4(a) and S5, we solved equations (1) and (2) simultaneously for μ and η using the SciPy fsolve tool⁴ in Python. Calculated changes in shear modulus ($\Delta\mu$) and dynamic viscosity ($\Delta\eta$) of Ti₃C₂ film during adsorption of water are shown in Figure S10(a) and S10(b) respectively. Both shear modulus and viscosity increase with RH, particularly for RH > 70%. From 0-85% RH, shear modulus increases by ~25 GPa at the 9th harmonic, corresponding to ~4-5% of the total elastic modulus (Young's modulus) of Ti₃C₂ film (~500-600 GPa) estimated by others using molecular dynamics and first principles calculations⁵⁻⁷. The increase in shear modulus is consistent with findings of Come et al. who showed that elastic modulus of Ti₃C₂ film increased by a factor of ~2 when intercalated water content increased from 12.5-100%. Stiffening of Ti₃C₂ film was attributed to possible formation of highly ordered water layers between Ti₃C₂ sheets⁸. The significant energy dissipation observed at 7th and 9th harmonics in Figure S5 is a result of increasing film viscosity. Water accumulation on Ti₃C₂ domain edges and van der Waals interactions between water and hydrophilic terminations likely resulted in adsorption of weakly-bound water which contributed to damping of the crystal oscillation⁹, resulting in higher effective viscosity.

It is worth noting that changes in $\Delta\mu$ and $\Delta\eta$ increased with harmonic number, which suggests that changes in viscoelastic behavior did not occur uniformly throughout the Ti₃C₂ film. The penetration depth (δ) at which amplitude of the acoustic wave decreases to 1/e of its value at the crystal surface is $\delta = \sqrt{\eta/2\pi f\rho}$ ¹⁰. By comparing $\Delta\mu$ and $\Delta\eta$ response at different harmonics, it is possible to estimate depth-dependence of the viscoelastic response. Figures S11(a) and S11(b) show $\Delta\mu$ and $\Delta\eta$ response vs. crystal harmonic number and estimated acoustic penetration depth respectively ($\delta = 0$ corresponds to the crystal surface). Viscoelastic changes decrease exponentially with distance from the crystal surface. This is expected for a viscoelastic film since damping results in decreased oscillation amplitude and acceleration as distance from the crystal increases.

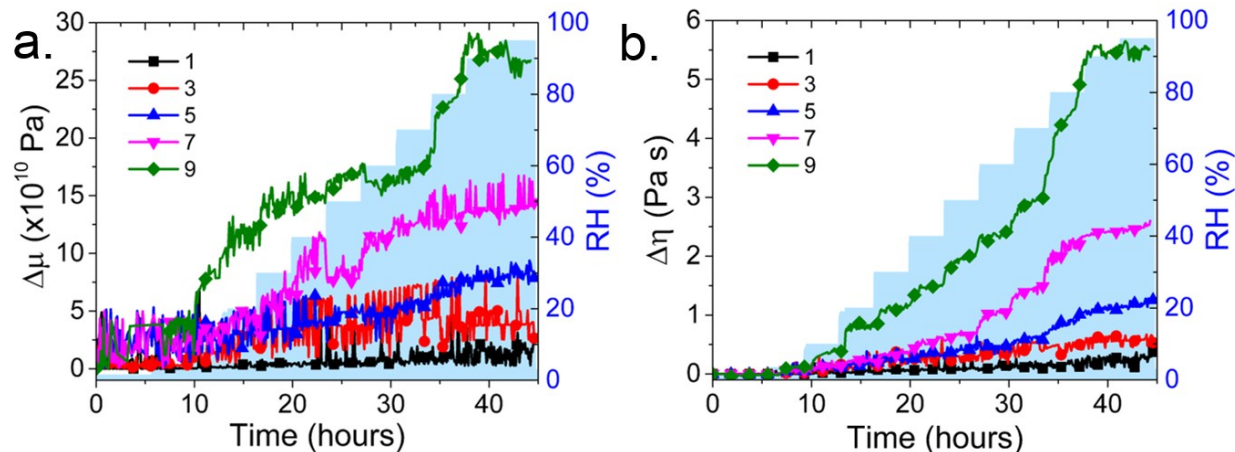


Figure S10. Changes in shear modulus ($\Delta\mu$, a) and viscosity ($\Delta\eta$, b) of Ti_3C_2 film exposed to changing RH levels (blue, right axis). Values of $\Delta\mu$ and $\Delta\eta$ were calculated using the viscoelastic Voigt model described by Voinova et al.¹.

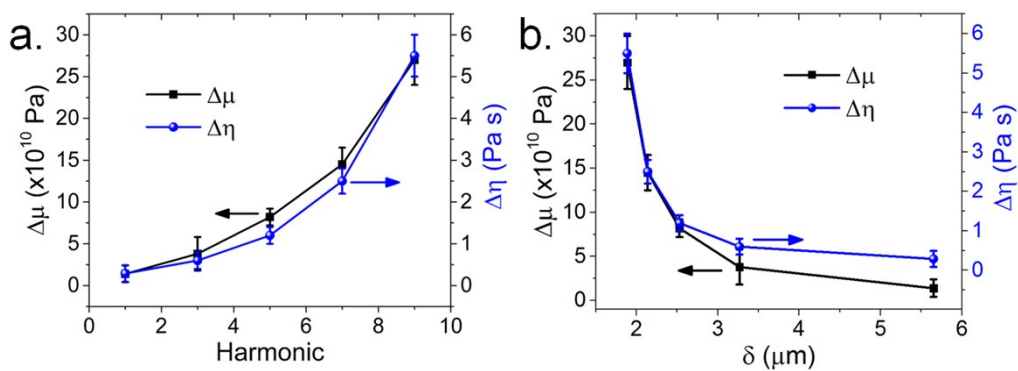


Figure S11. Changes in shear modulus ($\Delta\mu$, black left axis) and viscosity ($\Delta\eta$, blue right axis) of Ti_3C_2 film when RH was increased from 1.5% to 95% RH plotted against (a) crystal harmonic and (b) penetration depth of the acoustic wave (δ).

Sensitivity of RH-sensing modes

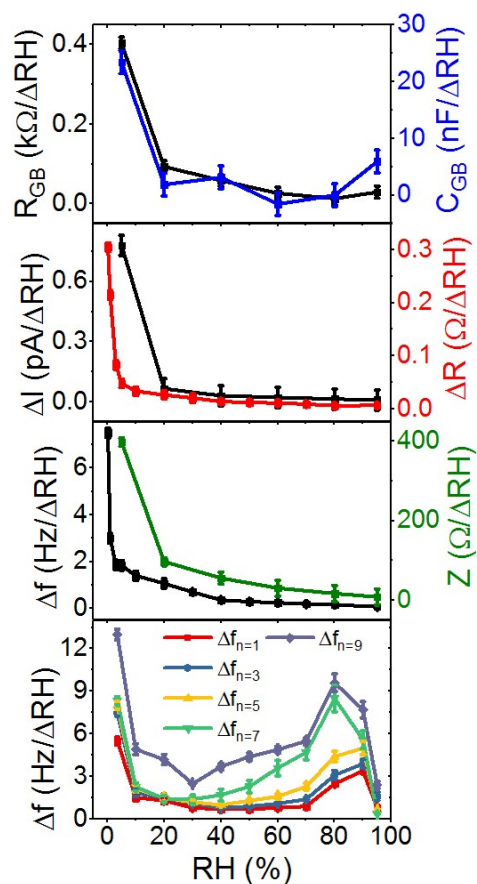


Figure S12. Sensitivity of each sensing mode: R_{GB} (grain boundary), C_{GB} (grain capacitance), I (current), ΔR (DC resistance), Δf_n (multi-harmonic QCM frequency shift, $n=1,3,5,7,9$) in terms of sensing mode units/ ΔRH .

References

1. Voinova, M. V.; Rodahl, M.; Jonson, M.; Kasemo, B., Viscoelastic Acoustic Response of Layered Polymer Films at Fluid-Solid Interfaces: Continuum Mechanics Approach. *Physica Scripta* **1999**, *59* (5), 391.
2. Hu, M.; Li, Z.; Zhang, H.; Hu, T.; Zhang, C.; Wu, Z.; Wang, X., Self-Assembled Ti₃C₂T_x Mxene Film with High Gravimetric Capacitance. *Chemical Communications* **2015**, *51* (70), 13531-13533.
3. Ling, Z.; Ren, C. E.; Zhao, M.-Q.; Yang, J.; Giammarco, J. M.; Qiu, J.; Barsoum, M. W.; Gogotsi, Y., Flexible and Conductive Mxene Films and Nanocomposites with High Capacitance. *Proceedings of the National Academy of Sciences* **2014**, *111* (47), 16676-16681.
4. Jones, E.; Oliphant, T.; Peterson, P., {Scipy}: Open Source Scientific Tools for {Python}. **2014**.
5. Guo, Z.; Zhou, J.; Si, C.; Sun, Z., Flexible Two-Dimensional Ti_{N+1}C_N (N= 1, 2 and 3) and Their Functionalized Mxenes Predicted by Density Functional Theories. *Physical Chemistry Chemical Physics* **2015**, *17* (23), 15348-15354.
6. Kurtoglu, M.; Naguib, M.; Gogotsi, Y.; Barsoum, M. W., First Principles Study of Two-Dimensional Early Transition Metal Carbides. *Mrs Communications* **2012**, *2* (4), 133-137.

7. Borysiuk, V. N.; Mochalin, V. N.; Gogotsi, Y., Molecular Dynamic Study of the Mechanical Properties of Two-Dimensional Titanium Carbides Ti_nC_{2n-1} (Mxenes). *Nanotechnology* **2015**, *26* (26), 265705.
8. Come, J.; Xie, Y.; Naguib, M.; Jesse, S.; Kalinin, S. V.; Gogotsi, Y.; Kent, P. R.; Balke, N., Nanoscale Elastic Changes in 2d Ti_3C_2Tx (Mxene) Pseudocapacitive Electrodes. *Advanced Energy Materials* **2016**, *6* (9).
9. Cho, N.-J.; Kanazawa, K. K.; Glenn, J. S.; Frank, C. W., Employing Two Different Quartz Crystal Microbalance Models to Study Changes in Viscoelastic Behavior Upon Transformation of Lipid Vesicles to a Bilayer on a Gold Surface. *Analytical Chemistry* **2007**, *79* (18), 7027-7035.
10. Speller, N. C.; Siraj, N.; Regmi, B. P.; Marzoughi, H.; Neal, C.; Warner, I. M., Rational Design of Qcm-D Virtual Sensor Arrays Based on Film Thickness, Viscoelasticity, and Harmonics for Vapor Discrimination. *Analytical Chemistry* **2015**, *87* (10), 5156-5166.